In Situ Synchrotron X-ray Spectroscopy of Ruthenium Nanoparticles Modified with Selenium for an Oxygen Reduction Reaction

ARTICLE *in* THE JOURNAL OF PHYSICAL CHEMISTRY C · OCTOBER 2007

Impact Factor: 4.77 · DOI: 10.1021/jp072581l

7 AUTHORS, INCLUDING:

Junji Inukai
University of Yamanashi
100 PUBLICATIONS **1,725** CITATIONS
SEE PROFILE

Andreas Menzel
Paul Scherrer Institut
139 PUBLICATIONS **2,258** CITATIONS
SEE PROFILE

Vladimir Komanicky
Pavol Jozef Šafárik University in Košice
47 PUBLICATIONS **686** CITATIONS
SEE PROFILE

Hoydoo You
Argonne National Laboratory
162 PUBLICATIONS **3,564** CITATIONS
SEE PROFILE

In Situ Synchrotron X-ray Spectroscopy of Ruthenium Nanoparticles Modified with Selenium for an Oxygen Reduction Reaction

Junji Inukai,[†,§] Dianxue Cao,[†] Andrzej Wieckowski,[†] Kee-Chul Chang,[‡] Andreas Menzel,[‡,||] Vladimir Komanicky,[‡,⊥] and Hoydoo You*[,‡]

Department of Chemistry, University of Illinois at Urbana-Champaign, Urbana, Illinois 61801, Materials Science Division, Argonne National Laboratory, Argonne, Illinois 60439, Clean Energy Research Center, University of Yamanashi, Kofu, Yamanashi, 400-0032 Japan

Received: April 2, 2007; In Final Form: July 9, 2007

We used in situ Se K-edge X-ray spectroscopy to characterize Ru nanoparticles chemically modified with submonolayers of selenium (Se/Ru) [Cao et al. *J. Electrochem. Soc.* **2006**, *153*, A869]. X-ray powder diffraction verified that the Se/Ru catalyst had metallic Ru cores. The in situ X-ray absorption near edge structure taken at the open circuit potential showed that there were both elemental and oxidized selenium on the as-prepared Se/Ru samples. All selenium oxide was reduced to the elemental form of selenium by applying negative potentials. By applying positive potentials, selenium was subsequently reoxidized. The analysis of the extended X-ray absorption fine structure shows the appearance of selenium hydration ($Se-OH_2$) in a deaerated solution, which was not observed during the oxygen reduction reaction. We present evidence that Se-free Ru atoms play an important role in the ORR activity of the Se/Ru catalyst studied in this paper.

Introduction

Direct methanol fuel cells (DMFC) show great potential as a future power source for portable electronics. By using methanol directly as fuel, issues relating to hydrogen storage and production can be bypassed, simplifying and reducing the weight of the fuel supply component of the fuel cell power source. However, DMFC suffers from low efficiency and poor power performance. These disadvantages would increase the weight of the fuel cell stack compared to similarly rated hydrogen fuel cells, and might consequently prevent its wide commercialization.[1]

One of the major reasons behind the poor performance of DMFC is methanol crossover. Methanol readily enters and penetrates the polymer electrolyte membrane and reaches the platinum cathode, where it is oxidized. This results in wasted fuel and, more importantly, in reduced cell voltage. New selective cathode materials that are tolerant to methanol and yet have high activity for the oxygen reduction reaction (ORR) need to be developed to address the issue of reduced cell voltage in order to improve the efficiency of DMFC.

A ruthenium chalcogenide cluster material of the type Ru_xSe_y, first reported by Alonso-Vante and co-workers, has been attracting major attention as a platinum-free, methanol-tolerant cathode material.[2] Ru_xSe_y catalysts, synthesized from ruthenium carbonyl ($Ru_3(CO)_{12}$) and elemental selenium in organic solvent, have a high ORR activity, while being tolerant to methanol crossover. However, the role of Se in increasing the ORR activity of Ru is not fully understood.

This present work was motivated by the need for obtaining more details on ORR on Se/Ru materials (see below) through in situ spectroscopic measurements. Another motivation was to track oxidative removal of surface Se (from the Se/Ru catalyst) at high electrode potentials. This work is a continuation of the "proof-of-concept" approach to the ORR Se/Ru catalysis reported previously.[3] It supports our previous finding that the Se is present on the Ru surface during ORR and that active catalysts can be obtained by spontaneous deposition or surface chemical reaction tactics.[3] In terms of the ORR activity, the Se/Ru catalysts we produce are equivalent to the Ru_xSe_y material reported by Alonso-Vante et al.,[2] as highlighted previously.[3−5]

In the cited study,[3] we also found that there was a difference between smooth Ru disk electrodes covered by Se and the nanoparticle Se/Ru material in terms of reactivity toward oxygen reduction. Apparently, the smooth Ru disks similarly modified by Se showed a lower ORR activity, whereas the Se-modified Ru nanoparticles showed significant enhancement in activity.

Alonso-Vante and co-workers made a series of X-ray investigations[6,7] on the Ru_xSe_y samples prepared using the cluster method[2]. They studied in situ the Ru K-edge with several chalcogenide modifiers and have shown that the nanoparticles have Ru core with a triangular co-ordination.[6] In another study, where ex situ Se K-edge and powder diffraction measurements were combined, they also proposed that Ru is the active center for the ORR reaction, whereas Se acts to prevent formation of RuO_2, which is inactive for ORR.[7]

In this study, we examined Se K-edge in situ in a thin-layer glancing-angle reflection geometry (see the Experimental Section). The primary focus of this study is to better understand the still contradicting roles of Se in (i) improving the ORR activity of Ru nanoparticles while (ii) poisoning the flat Ru disk surface.[3] X-ray synchrotron fluorescence spectroscopy data at the Se K-edge were taken for two types of Ru samples that were modified with different amounts of Se. On the basis of the preparation method, we expect that all Se atoms cover the

* To whom correspondence should be addressed.
† University of Illinois at Urbana-Champaign.
‡ Argonne National Laboratory.
§ University of Yamanashi.
|| Current Address: Paul Scherrer Institute, CH-5232 Villigen PSI, Switzerland.
⊥ Current Address: Institute for Experimental Physics, SAS Kosice, Slovakia.

10.1021/jp072581l CCC: $37.00
Published on Web 10/18/2007

outer surface of the Ru nanoparticles. Therefore, the Se K-edge spectroscopy is expected to be an ideal method to probe the role of Se in the Se/Ru materials as catalysts for oxygen reduction reaction.

Experimental Section

Se/Ru Nanoparticle Synthesis. As-received Ru black (Alfa Aesar, 99.9%) was reduced at 503 ± 5 K for 1 h under hydrogen (UHP) flow using a home-designed apparatus. The reduced Ru black was cooled to room temperature under protection of hydrogen gas, which was then replaced by argon (UHP). A suspension of as-received Se powder from 10 to 50 mg (Alfa Aesar, 200 mesh) in xylene (Fisher Scientific, certified ACS), previously dried using molecular sieves (4A, Aldrich) for 1 week and purged with Ar for 30 min, was injected into the flask containing the reduced Ru black of 150 mg: the Se loadings of 6.3, 11.8, 16.7, 21.1, and 25.0 wt % were thus obtained. The mixture was heated to the boiling temperature of the solvent (~415 K) and was refluxed for 24 h under slow Ar bubbling. The resulting Se/Ru nanoparticles were separated from the solvent by centrifuging. The specimens were subsequently washed with anhydrous ethyl ether (Fisher Scientific, certified ACS) six times and finally dried under vacuum for 2 h. The samples with 16.7 and11.8 wt % loadings of Se were named "sample A" and "sample B", respectively. Our X-ray powder diffraction data (to be discussed later in the paper) gave an average of 10 nm for the Ru core size after nanoparticles are modified by Se. If we assume that the Ru particles are round balls that are 10 nm in diameter and that the Se atoms form a monolayer on the particles, we estimate that roughly 90 and 60% of the Ru surface was covered with Se in samples A and B, respectively.

Rotating Disc Electrode Measurements. The rotating disc electrode measurements were carried out following the same procedure as reported previously.[3] To prepare Se/Ru nanoparticle catalyst electrodes, a suspension of 2.5 mg mL^{-1} of the catalyst in Millipore water was prepared by sonication for 30 min. About 4.2 μL of the catalyst suspension was placed onto a Au rotating disk electrode (RDE) with a diameter of 3 mm and dried in air at room temperature for 2 h to give a catalyst loading of 150 μg cm^{-2}. The thin layer of nanoparticles was thus immobilized on the RDE surface. The RDE measurements were carried out in a 0.1 M H_2SO_4 solution saturated with O_2 in a standard three electrode electrochemical cell controlled by a Autolab PGSTAT100 potentiostat (Eco Chemie). The reference electrode was Ag/AgCl (3M KCl) placed in a Luggin capillary and calibrated versus the reversible hydrogen electrode (RHE) before carrying out ORR. All potentials in this work are reported versus the RHE.

X-ray Powder Diffraction. Se/Ru nanoparticles were compacted into a pellet form and placed on a four-circle diffractometer with a rotating-anode X-ray source (Rigaku, Cu Kα line) for powder diffraction measurements. The samples were stored in air before the measurement. To prevent further oxidization of the nanoparticles in the presence of X-rays, the pellet was placed inside a polypropylene bag that was continually flushed with argon during the data collection.

X-ray Fluorescence Spectroscopy. X-ray fluorescence spectra of the Se K-edge were acquired at a bending magnet beamline (12-BM) at the Advanced Photon Source, Argonne National Laboratory. Se K-edge data were collected using a Si(111) double-crystal monochromator (energy resolution $\Delta E/E = 14.1 \times 10^{-5}$) and double Pt mirrors for focusing and harmonic rejection. All data were taken in the fluorescence mode using a Vortex multi-cathode X-ray detector. A 5-μm thick gold foil and a 4-μm thick platinum foil were used as filters in front of the detector to reduce the elastic X-ray intensity, and a single-channel analyzer was used to narrow the detection energy window tightly around the Se Kα fluorescence.

Before analyzing the X-ray spectroscopy data, the background was subtracted using the AUTOBK algorithm.[8] Data reduction and analysis were performed using Athena as a front-end.[9] The Se K-edge spectra were calibrated by defining the first inflection point of a Se foil XANES spectrum as 12,858 eV. The single-scattering backscattering amplitude and the phase-shift functions used in the analysis were calculated using FEFF8.[10] Theoretical least-squares fits of the spectra to the EXAFS equation were performed in R space over a 1.2−3.0 Å range using "ifeffit" with Artemis as a front-end.[11] The amplitude reduction term was calculated theoretically using FEFF8, and the Debye−Waller (DW) factors were fixed to reduce the number of variables used in the fitting.

For in situ X-ray measurements under potential control, Se/Ru nanoparticles were suspended in water and a drop of suspension was dried on a glassy carbon disk, with the catalyst loading of 15 μg cm^{-2}. A thin layer of Nafion solution was then dried on top of the nanoparticles to fix them to the carbon disk. The samples were then transferred into a thin layer X-ray cell and covered with Kapton or polypropylene film for the measurement in 0.1 M H_2SO_4 electrolyte, either deaerated by argon or saturated with oxygen. In the oxygenated solution, the XAFS data were obtained in situ during the ORR. An Ag/AgCl (3M KCl in gel) electrode placed in the Luggin capillary was used as a reference. The reference electrode was placed on a side junction of the cell to prevent chloride ion contamination during the experiment.

The X-ray beam was at a glancing-angle incidence to the surface of the polished carbon disk to maximize fluorescence and to minimize the elastic scattering. An initial energy scan was taken at the open circuit potential (OCP) in the deaerated solution under argon atmosphere. After the first scan on the as-prepared sample, the electrode potential was subsequently set at 30 mV. The sample was then "activated" by the potential cycling between 30 mV and 950 mV four times at the scan rate of 20 mVs^{-1}. After cycling, the solution was flushed at OCP to remove any dissolved Se ions. The X-ray fluorescence signal did not change before and after this activation process, indicating that no significant Se dissolution took place. From 30 mV, the electrode potential was changed stepwise in the positive direction, and the XAFS spectra were obtained at different potentials. When XAFS measurements were carried out during the ORR, oxygen was used, instead of argon, to produce O_2-saturated solutions. During the in situ experiments under electrode potential control, 5 min was allowed after each potential change for equilibration.

Results and Discussion

ORR Measurements using RDE. Before the XAFS experiments, the ORR activity on the Se/Ru samples was examined. In Figure 1, the ORR data using the RDE in O_2-saturated 0.1 M H_2SO_4 are presented. The electrode was voltammetrically "pre-cycled" between 30 and 1200 mV[3], and the current−potential curves were obtained at 20 mV s^{-1} and 1600 rpm. This pre-cycling helped the excess Se in the form of Se oxides to dissolve at higher potentials and to reduce the oxides at lower potentials. The effect of pre-cycling on the Se/Ru catalyst was reported previously.[12] The oxygen reduction current commenced at 900 mV on all catalysts with a diffusion limiting current of

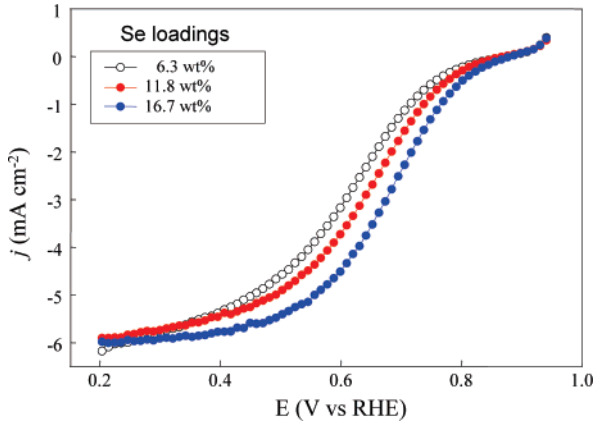

Figure 1. Current−potential curves obtained during ORR on the Se/Ru catalyst. White, red (sample B), and blue (sample A) represent Se/Ru prepared with Se loading of 6.3, 11.8, and 16.7 wt %, respectively. RDE measurements were carried out in an O_2-saturated 0.1 M H_2SO_4 solution at 20 mVs^{-1} at 1600 rpm. The Se/Ru loading on RDE is 150 $\mu g\ cm^{-2}$.

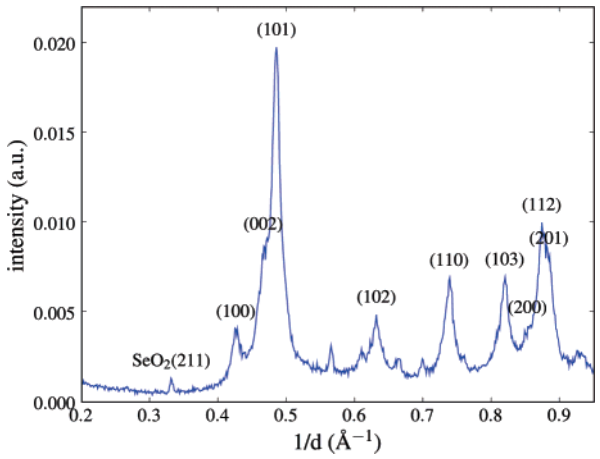

Figure 2. X-ray powder diffraction pattern of Ru nanoparticles chemically modified with Se (sample A). Ru peaks dominate the diffraction pattern with a small peak at 0.33 $Å^{-1}$ identified as due to SeO_2(211).

6 mA cm^{-2}. As the amount of Se on the catalysts increased from 6.3 to 16.7 wt %, the ORR activity increased. At Se loadings higher than 25.0 wt %, only a small increase in the ORR activity was observed (not shown). For the catalyst with 16.7 wt % of Se loading (sample A) the activity was identical to that reported in the previous study.[3]

X-ray Powder Diffraction. The samples were characterized using in-house powder-diffraction measurements before the in situ synchrotron X-ray measurements. The powder diffraction pattern on the Se/Ru (sample A) from the 12 kW rotating-anode X-ray source is shown in Figure 2. Aside from a small peak at 0.33 $Å^{-1}$ probably due to a small amount of SeO_2, peaks from hexagonally close-packed metallic ruthenium dominate the diffraction pattern. No peaks from elemental Se were detected; thus, elemental Se should be homogeneously dispersed on the Ru nanoparticles.[12] The powder diffraction of sample B yielded similar results.

Although the Ru nanoparticles were kept in air after syntheses, peaks corresponding to RuO_2 were not detected. Therefore, the core of Ru nanoparticles remained metallic. We believe that Se is protecting Ru against oxidation, in agreement with the studies by Dassenoy et al.[13] and Zaikovskii et al.[14] Our recent XPS data also clearly showed the effect of Se preventing Ru from oxidation on Se/Ru.[12] The average particle

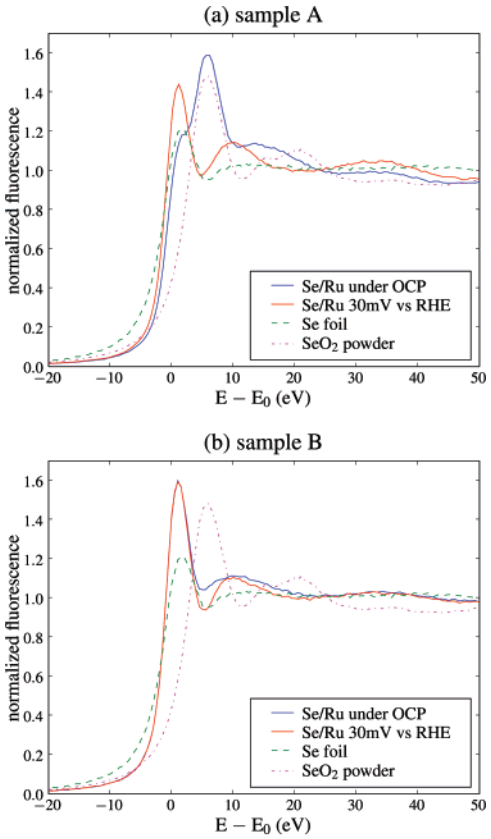

Figure 3. Comparison of the Se edge XANES of samples (a) A and (b) B in 0.1M H_2SO_4 before and after activation. The peak position of the white line for Se/Ru at OCP coincides with that for SeO_2 powder, suggesting that the Se^{4+} is present in the sample. After activation at 30 mV, Se is reduced to an elemental state. XANES data for sample B show that the Se is much less oxidized in this sample compared to sample A.

size was ∼10 nm as estimated from the full width half-maximum of the (110) peak using the Debye−Scherrer equation.

X-ray Absorption Near Edge Spectroscopy (XANES). Figure 3 shows XANES scans of the nonactivated and activated samples A and B. Reference spectra of Se and SeO_2 powder samples were also measured and shown for comparison. Electronic transitions at the Se K-edge occur from 1s into unoccupied 4p states. The edge position is sensitive to the oxidation state of Se. It increases by 4 and 6 eV from the Se^0 edge position for Se^{4+} and Se^{6+}, respectively.[15] The white-line intensity also increases with the unoccupied density at the 4p states and, consequently, with the extent of oxidation. XANES data of sample A measured at OCP are shown in Figure 3a. The peak position nearly overlaps the peak for the reference SeO_2 powder, and the intensity of the white line is very large. Therefore, we conclude that SeO_2 existed on sample A before activation. SeO_2 clusters must be very small and dispersed because the SeO_2 peaks in the X-ray powder diffraction pattern were almost negligible compared to the Ru peaks (Figure 2). It is notable that the XANES data for sample B (Figure 3b) with the smaller Se loading shows the absence of a SeO_2-like spectrum. Therefore, the small amount of SeO_2 on sample A might not be attached to Ru. After activation and cell flushing, we obtained similar XANES data for both samples A and B, showing no SeO_2 character. Therefore, the activation process dissolved the excess SeO_2 at high electrode potentials and reduced the remaining selenium oxides to metallic Se^0 at low potentials. This conclusion is supported by our ex situ XPS results obtained by using equivalent samples.[12] The linear

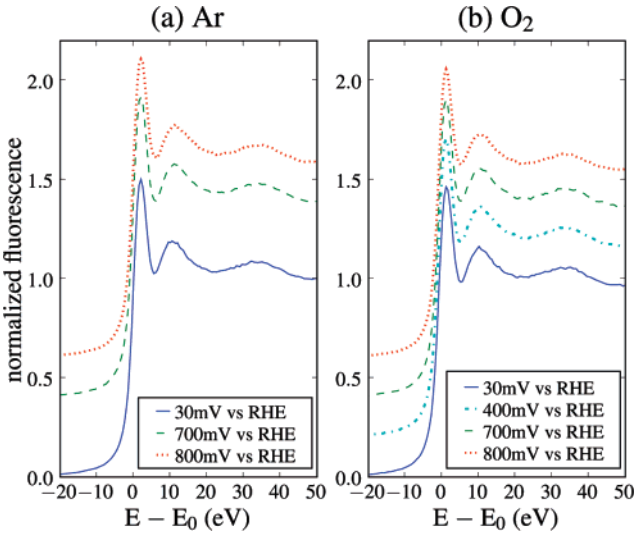

Figure 4. In situ Se edge XANES of Sample A in (a) Ar and (b) O_2 saturated 0.1 M H_2SO_4 as the electrode potential is raised. Each scan is offset by 0.1 in the vertical scale to facilitate comparison. For potentials up to 800 mV, no change in XANES was observed for either solution.

combination fits of XANES data of Se on samples A and B using spectra of powder Se and SeO_2 gave poor results. Since XANES spectra are sensitive not only to the oxidation states but also to the geometrical arrangements of atoms and the local electronic structure, the poor linear combination suggests that Se in the Se overlayer on Se/Ru are geometrically and electronically different from that in Se bulk. The detailed structure of Se in the Se overlayer on Ru will be later discussed based on our EXAFS results.

Under the electrode potential control, the XANES data for samples A and B did not change up to 800 mV either in deaerated or in oxygen-saturated solutions, as shown in Figure 4. This agrees with our previous CV measurements, where the oxidation current started at 850 mV.[3,12]

As shown in Figure 5, Se started to oxidize when the electrode potential was jumped from 800 to 900 mV for both samples A and B. The series of scans show two isosbestic points at +4 and +10 eV from the edge. This means that SeO_2 was the only oxidized species transformed from Se during the oxidation. The total intensity of the XANES peaks showed only a small change, meaning once the catalysts were activated, the reoxidized Se remained on the Ru surface.

Extended X-ray Absorption Fine Structure (EXAFS). In situ EXAFS scans were taken for sample A under potential control to study the local environments of Se in deaerated and oxygen-saturated solutions. Figure 6 shows a Fourier transform (FT) of the EXAFS spectra at different potentials measured in the solutions. The main peaks due to Se−Ru and Se−Se bonds appear at 2.3 Å. A Se−Ru bond is seen to be split due the Ramsauer−Townsend resonance, with a smaller side peak shifted to the left of the main peak at 2.0 Å.[16] Such split is more obvious in the spectra obtained in an O_2-saturated solution than in deaerated solutions. For the spectra taken with a deaerated solution, an extra feature rapidly grows at 1.4 Å. Because no anodic current was seen in the CV for Se/Ru until the electrode potential reached to 850 mV,[3] the side peak at 1.4 Å most likely originates from adsorption of electrochemically neutral species. We tentatively assign this peak to Se−O, formed by the adsorption of water molecules on Se at anodic potentials. The distance of 1.4 Å is consistent with the Se−O distance. The growth of the Se−O bond could be explained in

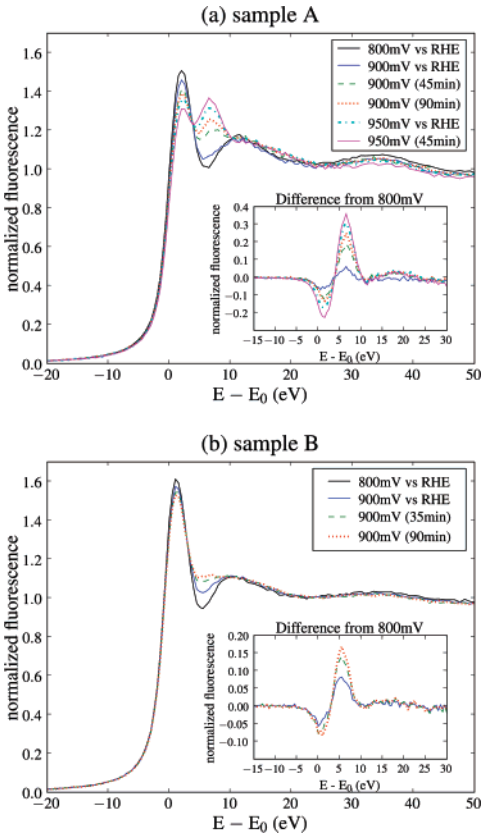

Figure 5. In situ Se edge XANES of samples (a) A and (b) B in the deaerated 0.1M H_2SO_4 solution as potential was raised above 800 mV. From 900 mV, Se started to be oxidized.

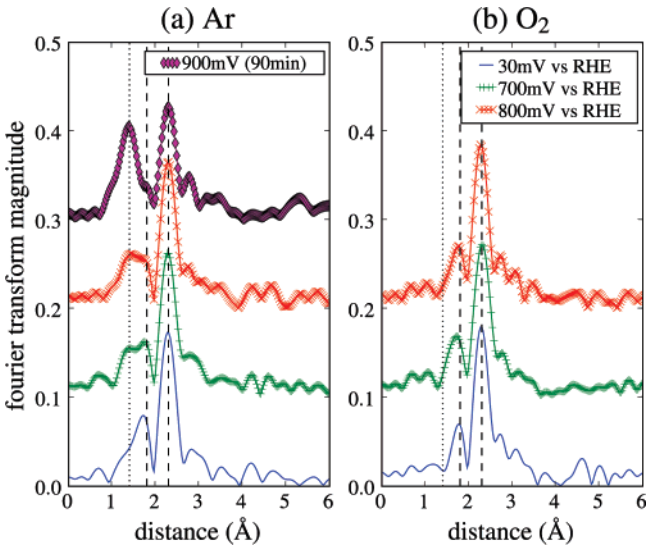

Figure 6. Fourier transformed in situ EXAFS spectra of sample A at different potentials for (a) deaerated and (b) O_2-saturated solutions. The dashed lines show expected positions of the split peaks for the Se−Ru bond due to the Ramsauer−Townsend resonance. The dotted lines show expected peak positions for the Se−O bond. Se−Se bond distances produce a peak that overlaps with the higher order Se−Ru peak.

terms of the potential-dependent reorientation of water molecules as the surface charge changes from negative to positive, which has been reported in the in situ infrared spectroscopy study of a gold electrode surface in perchloric acid.[17] In the spectra obtained in O_2-saturated solutions, no such $Se-OH_2$ features were observed. The reason for the absence of the Se−O bond during the ORR is not clear at the moment. It has been reported

TABLE 1: Bond Distances (*R*) and Coordination Numbers (CN) Obtained by Fitting the Se EXAFS Data

		electrode potential (RHE) in argon			electrode potential (RHE) in O_2		
bond type		30 mV	700 mV	800 mV	30 mV	700 mV	800 mV
Se−Ru	*R* (Å)	2.39 ± 0.01			2.44 ± 0.01		
	CN	1.51 ± 0.26	1.50 ± 0.29	1.38 ± 0.31	1.81 ± 0.13	2.02 ± 0.15	2.11 ± 0.16
Se−Se	*R* (Å)	2.60 ± 0.02	2.61 ± 0.02	2.60 ± 0.03	2.90 ± 0.05	2.87 ± 0.04	2.88 ± 0.03
	CN	1.13 ± 0.34	1.05 ± 0.35	1.02 ± 0.35	0.33 ± 0.25	0.51 ± 0.28	0.64 ± 0.31
Se−O	*R* (Å)	1.70 ± 0.03				Se−Se DW: 0.005 Å^{-2}	
	CN	0.28 ± 0.15	0.27 ± 0.18	0.34 ± 0.18		all other DW: 0.005 Å^{-2}	
E_0		1.81 ± 0.89			3.48 ± 0.47		
R factor		0.049	0.050	0.041	0.042	0.018	0.022
Se−Ru	*R* (Å)	2.41 ± 0.01			2.44 ± 0.01		
	CN	1.63 ± 0.27	1.67 ± 0.31	1.56 ± 0.33	1.84 ± 0.13	2.05 ± 0.15	2.14 ± 0.17
Se−Se	*R* (Å)	2.59 ± 0.04	2.62 ± 0.06	2.60 ± 0.06	2.90 ± 0.07	2.88 ± 0.04	2.89 ± 0.07
	CN	1.06 ± 0.66	1.00 ± 0.74	0.90 ± 0.77	0.48 ± 0.42	0.93 ± 0.48	1.10 ± 0.53
Se−O	*R* (Å)	1.70 ± 0.04				Se−Se DW: 0.01 Å^{-2}	
	CN	0.23 ± 0.14	0.20 ± 0.17	0.27 ± 0.17		all other DW: 0.005 Å^{-2}	
E_0		2.13 ± 0.79			3.51 ± 0.47		
R factor		0.064	0.051	0.040	0.044	0.016	0.022
Se−Ru	*R* (Å)	2.42 ± 0.01			2.43 ± 0.01		
	CN	1.72 ± 0.30	1.67 ± 0.36	1.58 ± 0.37	1.85 ± 0.16	2.10 ± 0.17	2.19 ± 0.19
Se−Se	*R* (Å)	2.59 ± 0.09	2.63 ± 0.09	2.59 ± 0.09	2.89 ± 0.15	2.89 ± 0.05	2.91 ± 0.05
	CN	1.36 ± 1.75	1.83 ± 1.88	1.53 ± 2.11	0.61 ± 0.1.03	1.99 ± 1.11	2.16 ± 1.21
Se−O	*R* (Å)	1.70 ± 0.04				Se−Se DW: 0.02 Å^{-2}	
	CN	0.23 ± 0.16	0.21 ± 0.19	0.28 ± 0.19		all other DW: 0.005 Å^{-2}	
E_0		2.50 ± 0.90			3.50 ± 0.50		
R factor		0.108	0.076	0.074	0.049	0.015	0.023

that there is an interaction between Ru and O during the ORR on Ru_xSe_y.[6,7] This Ru−O interaction might have some influence on the chemical state of Se to make Se−O interaction weaker during ORR on Se/Ru.

The Se−Se and Se−Ru bond distances and the coordination numbers (CN) obtained from the EXAFS spectra are shown in Table 1. For the EXAFS fitting, the reported CN is the product of the actual coordination number with the passive electron reduction factor (S_0^2) of 0.911 calculated with FEFF8. We used the calculated value due to the absence of reliable standards. The fitting interval of 2.5−10.5 Å^{-1} in the k-range of the EXAFS spectrum and 1.2−3.2 Å in the R-range of the Fourier transformed EXAFS spectrum gives only 10 independent points. To increase the number of independent parameters, we used three spectra taken at 30, 700, and 800 mV to get a total of 30 independent points (since we found no significant differences among the three spectra). Relaxing the Se−Ru and Se−O DW factors did not improve the fit significantly, therefore, they were fixed at 0.005 Å^{-2}. On the other hand, the Se−Se DW factor had a large effect on the overall fit; thus, we used three values for the Se−Se DW, 0.005, 0.01, and 0.02 Å^{-2}. The Se−O bond was used for fitting in the deaerated solution data set. On the other hand, the Se−O bond was excluded for the data set obtained in an O_2-saturated solution because using the bond did not improve the fits. The maximum number of independent variables used in our fit was 15. An example of the fitting results for the sample under the O_2-saturated solution at 700 mV is shown in Figure 7.

The Se−Ru CN is expected to be 3 for an ideal geometry of Se sitting on the hollow Ru sites. The obtained number of ∼2 (Table 1) is reasonable if we assume Se is also at on-top and bridge sites. EXAFS spectra under O_2-saturated solution show that the Se−Ru coordination number is virtually unchanged as the applied potential is increased. These results suggest that the average Se−Ru bonding geometry is stable during ORR.

The Se−Se CNs are expected to be 4 or 6 for an ideal square geometry or a hexagonal geometry, respectively, if we have a full monolayer coverage as assumed in the coverage calculations. However, the CNs obtained by fitting are less than 2, with a very large deviation. Also note that the Se−Se bond distances are larger than ∼2.3 Å (ascribed to the elemental Se). It is clear that the Se layers are different from the ideal compact monolayers. A strong correlation between the DW factor and the CN found in the fit indicates a large static disorder of Se atoms on

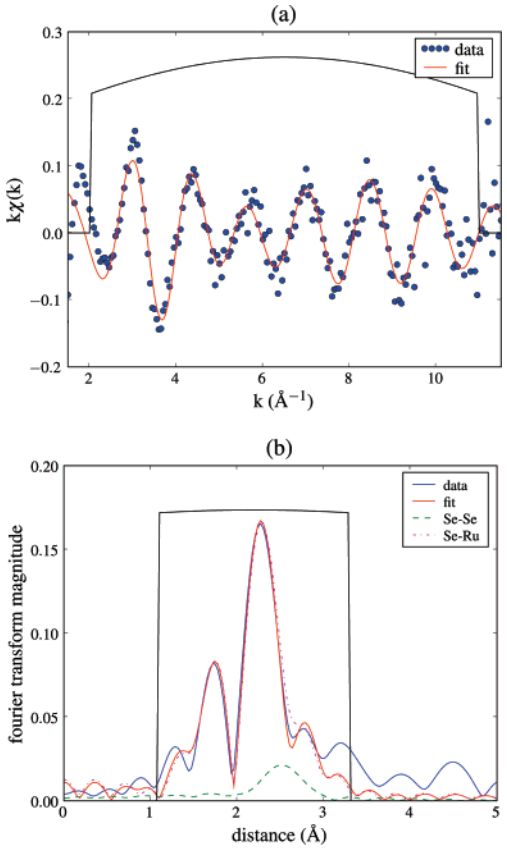

Figure 7. (a) In situ *k*-weighted EXAFS spectra of sample A at 700 mV under O_2 saturated solution and (b) its Fourier transform. Se−Se DW was set to 0.05 Å^2. Fits for Se−Se and Se−Ru bonds were limited to the first shells over 1.2 to 3.2 Å distance range (marked by a rectangle) in the radial distribution function. The Se−Ru bond contribution to the fit dominates over that of the Se−Se bond. The contributions to the FT for each of the bonds in the fit are shown in (b).

the Ru surface. Increasing the Se−Se DW factor resulted in an increase in the Se−Se CN, albeit at the expense of the corresponding increase in uncertainties. The increase was seen in both deaerated and O_2-saturated solutions although it was more pronounced in the O_2-saturated solutions. Therefore, it is likely that the Se atoms form nonuniform, aperiodic structure on the Ru nanoparticle surface allowing some surface Ru atoms to be exposed to solution.[14] These Ru atoms remain metallic as previously reported by using XPS.[12] As has been established on Pt surfaces,[18,18,19] a strong correlation exists between the oxide formation and the inhibition of the ORR. The metallic Ru sites surrounded by Se atoms are expected to act as the active sites for ORR.[6,7,12,14]

The nonuniform aperiodic distribution is unique to nanoparticles whose surfaces are inhomogeneous due to presence of multiple facets and various defects. It was previously reported that the Se layers similarly deposited on well-prepared flat Ru surfaces inhibited the ORR rather than promoted it.[3] We conjecture that this is because a uniform and dense periodic layer of Se formed and effectively poisoned the flat Ru surface.

Conclusions

In situ synchrotron X-ray fluorescence spectroscopy measurements were carried out in order to monitor the oxidation state of Se and the change in Se environment in the Se/Ru nanoparticle catalyst during ORR (oxygen reduction reaction). Oxidized selenium was found at OCP in the as-prepared samples, but the selenium was completely reduced by applying a potential of 30 mV. Electrode potentials higher than 800 mV caused the Se to reoxidize.

EXAFS data show that the Se−Ru bond and CN (coordination numbers) are close to the values for Se atoms on 3-fold sites of Ru. On the contrary, the Se−Se CN values are considerably smaller than those for Se forming a compact layer, indicating a disorder. Analysis of the EXAFS data obtained in an O_2-saturated solution showed no evidence of Se−O bond formation during ORR, whereas that of the EXAFS data obtained in deaerated solutions indicated the formation of $Se-OH_2$.

Previous studies of Ru_xSe_y using the Ru edge EXAFS showed that the Ru surface site is the active center for ORR.[7] In our data, the disordered Se adlayers covered Ru particles, with some surface Ru atoms left to be exposed to solution. Those Ru atoms are metallic as reported using XPS.[12] The same mechanism for enhancement in ORR may apply both on Ru_xSe_y and Se/Ru.

Acknowledgment. This work was supported by the U.S. Department of Energy, Office of Basic Energy Sciences, Materials Science Division, and the use of the Advanced Photon Source was supported by the U.S. Department of Energy, Office of Basic Energy Sciences under Contract No. DE-AC02-06CH11357. This work was partially supported by the Army Research Office through the MURI Grant (DAAD19-03-1-0169) for fuel-cell research to Case Western Reserve University.

References and Notes

(1) Larminie, J.; Dicks, A. *Fuel Cell Systems Explained*, 2nd ed.; Wiley: Chicester, U.K., 2003.
(2) Alonso-Vante, N.; Tributsch, H.; and Solorza-Feria, O. *Electrochim. Acta* **1995**, *40*, 567.
(3) Cao, D.; Wieckowski, A.; Inukai, J.; Alonso-Vante, N. *J. Electrochem. Soc.* **2006**, *153*, A869.
(4) DOE Docket No. S-109,023 for Method of Making Chalcogen Catalysts for Polymer Electrolyte Fuel Cells, U.S. Ser. No. 11/443,809, filed May 31, 2006, by Choi et al.
(5) DOE Docket No. S-104,947 for Chalcogen Catalysts for Polymer Electrolyte Fuel Cell, U.S. Ser. No. 11/295,361, filed Dec. 5, 2005, by Zelenay et al.
(6) Alonso-Vante, N.; Malakhov, I. V.; Nikitenko, S. G.; Savinova, E. R.; Kochubey, D. I. *Electrochim. Acta* **2002**, *47*, 3807.
(7) Malakhov, I. V.; Nikitenko, S. G.; Savinova, E. R.; Kochubey, D. I.; Alonso-Vante, N. *J. Phys. Chem. B* **2002**, *106*, 1670.
(8) Newville, M.; Livins, P.; Yacoby, Y.; Stern, E. A.; Rehr, J. J. *Phys. Rev. B* **1993**, *47*, 14126.
(9) Ravel, B.; Newville, M. *J. Synchrotron Radiat.* **2005**, *12*, 537.
(10) Rehr, J. J.; Albers, R. C. *Rev. Mod. Phys.* **2000**, *72*, 621.
(11) Newville, M. *J. Synchrotron Radiat.* **2001**, *8*, 322.
(12) Lewera, A.; Inukai, J.; Zhou, W. P.; Cao, D.; Duong, H.; Alonso-Vante, N.; Wieckowski, A. *Electrochim. Acta* **2007**, *52*, 5759.
(13) Dassenoy, F.; Vogel, W.; Alonso-Vante, N. *J. Phys. Chem. B* **2002**, *106*, 12152.
(14) Zaikovskii, V. I.; Nagabhushana, K. S.; Kriventsov, V. V.; Loponov, K. N.; Cherepnova, S. V. Kvon, R. I.; Bönnemann, H.; Kochubey, D. I.; Savinova, E. R. *J. Phys. Chem. B* **2006**, *110*, 6881.
(15) Pickering, I. J.; Brown, G. E., Jr.; Tokunaga, T. K. *Environ. Sci. Technol.* **1995**, *29*, 2456.
(16) Rehr, J. J.; Booth, C. H.; Bridges, F.; Zabinsky, S. I. *Phys. Rev. B* **1994**, *49*, 12347.
(17) Ataka, K.; Yotsuyanagi, T.; Osawa, M. *J. Phys. Chem.* **1996**, *100*, 10664.
(18) Schmidt, T. J.; Stamenkovic, V.; Ross, P. N.; Markovic, N. M. *Phys. Chem. Chem. Phys.* **2003**, *5*, 400.
(19) Yano, H.; Inukai, J.; Uchida, H.; Watanabe, M.; Babu, P. K.; Kobayashi, T.; Chung, J. H.; Oldfield, E.; Wieckowski, A. *Phys. Chem. Chem. Phys.* **2006**, *8*, 4932, and references therein.